



ELSEVIER

Contents lists available at ScienceDirect

Journal of Fluids and Structures

journal homepage: www.elsevier.com/locate/jfs

Fluid forces acting on a cylinder undergoing streamwise vortex-induced vibrations

N. Cagney, S. Balabani*

Department of Mechanical Engineering, University College London, Torrington Place, London WC1E 7JE, UK

ARTICLE INFO

Article history:

Received 9 July 2015

Accepted 9 January 2016

Keywords:

Vortex-induced vibrations

Fluid forces

Fluid–structure interaction

ABSTRACT

This brief communication examines the fluid forces acting on a cylinder free to move in the streamwise direction throughout its response regime. The amplitude and phase of the unsteady drag coefficient are estimated from the displacement signals and a simple harmonic oscillator model. We examine the counter-intuitive reduction in vibration amplitude observed in streamwise vortex-induced vibrations (VIV) at resonance, which has remained one of the most poorly understood aspects of VIV. Our results show that it is not caused by a change in the phase of the fluid forcing with respect to the cylinder displacement, as suggested by previous researchers; instead, we show that there is a sudden decrease in the amplitude of the unsteady drag coefficient in this region. The possible cause of this result, relating to three-dimensionality in the wake, is briefly discussed.

© 2016 Published by Elsevier Ltd.

1. Introduction

The problem of Vortex-Induced Vibration (VIV) of circular cylinders in crossflow is relevant to a wide range of industrial structures, such as tall chimneys, bridges, heat exchangers, off-shore platforms and oil risers. It is a classical fluid–structure interaction problem; the vortices shed from the cylinder induce unsteady fluid forces, which cause the structure to vibrate; this motion in turn affects the wake and the vortex-induced forces. This results in a complex feedback loop between the flow field and the structure that is controlled by the fluid forces. When the predicted vortex-shedding frequency (the Strouhal frequency), $f_{St} = St U_0/D$ (where St is the Strouhal number, U_0 is the freestream velocity and D is the cylinder diameter) is close to the vibration frequency of the cylinder, f_x , the cylinder motion can cause the vortex-shedding to occur at f_x or a sub-harmonic instead of the Strouhal frequency, a phenomenon known as ‘lock-in’.

The structural response, wake mode and the presence of lock-in are controlled by the so-called ‘true’ reduced velocity (Cagney and Balabani, 2013c; Govardhan and Williamson, 2000; Aguirre, 1977), $U_r St/f^*$, where $U_r = U_0/f_n D$ is the conventional reduced velocity, f_n is the natural frequency measured in a still fluid, and $f^* = f_x/f_n$ is the frequency ratio. The ‘true’ reduced velocity (henceforth referred to simply as the reduced velocity) is equal to the ratio of the predicted shedding frequency to the actual response frequency, f_{St}/f_x . As the fluctuating drag occurs at twice the shedding frequency, lock-in is expected to occur in the streamwise direction (i.e. parallel to the flow) at $U_r St/f^* = 0.5$, and at $U_r St/f^* = 1$ in the transverse direction (i.e. normal to the flow). This is typically associated with a change in the arrangement of vortices in the wake (the ‘wake mode’) and an increase in the vibration amplitude, A (Williamson and Roshko, 1988; Morse and Williamson, 2009).

* Corresponding author. Tel.: +44 20 7679 7184.

E-mail address: s.balabani@ucl.ac.uk (S. Balabani).

<http://dx.doi.org/10.1016/j.jfluidstructs.2016.01.007>

0889-9746/© 2016 Published by Elsevier Ltd.

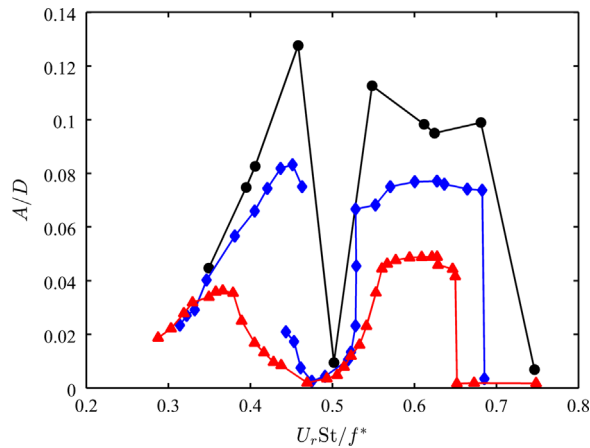


Fig. 1. Amplitude response of a cylinder undergoing streamwise VIV; Jauvtis and Williamson (2003) (pivoted cylinder, $m^* = 6.9$, $\zeta = 0.0014$, closed black circles); Aguirre (1977) ($m^* = 1.23$, $\zeta = 0.0018$, blue diamonds); Okajima et al. (2004) ($m^* \zeta = 0.195$, red triangles). These studies did not provide information on f^* , which is here assumed to remain equal to 1. The characteristic reduction in amplitude at $U_r St \approx 0.5$ is clear. (For interpretation of the references to color in this figure caption, the reader is referred to the web version of this paper.)

However, when the cylinder is free to move in the streamwise direction, the synchronisation between the unsteady drag force and the cylinder vibration coincides with a sudden reduction in amplitude (Aguirre, 1977; Jauvtis and Williamson, 2003; Okajima et al., 2004). This paradoxical feature of VIV can be seen in Fig. 1, which shows the results of three previous studies; the reduction in vibration amplitude at resonance is in contrast to almost all other forms of fluid–structure interaction and remains poorly understood (Konstantinidis, 2014).

Nishihara et al. (2005) measured the fluid forces acting on a cylinder forced to oscillate in the streamwise direction at $A/D = 0.05$ for a range of reduced velocities and found that near $U_r St / f^* = 0.5$ the phase difference between the cylinder displacement and the drag force changed such that energy was transferred from the cylinder (i.e. it was a damping force), which they proposed to be the cause of the counter-intuitive reduction in amplitude in this region. A similar argument was presented by Konstantinidis et al. (2005) and Konstantinidis and Liang (2011), who examined the wake of a cylinder in pulsating flow and observed a change in the phase of the vortex-shedding near $U_r St / f^* = 0.5$. However, Morse and Williamson (2009) showed that the fluid force will always provide negative excitation (i.e. a damping force) if the cylinder is forced to oscillate at an amplitude above which it would oscillate in the free-vibration case. Konstantinidis and Liang (2011) also note this issue, pointing out that the forced oscillation experiments do not take into account the fact that the phase of the drag force with respect to the cylinder displacement will depend on the vibration amplitude. In light of this, the findings of Nishihara et al. (2005) could be said to be known a priori and the cause of the reduction in A/D near $U_r St / f^* = 0.5$ remains unclear.

In order to fully understand the complex coupling between the wake in the structural motion, knowledge of the fluid forces acting on the cylinder is required. However, it is often difficult in practice to accurately measure the forces acting on a freely oscillating body; for many experimental configurations it may not be possible to attach strain gauges to the body or its supports, and the measurements may be inaccurate when the amplitude of the forces is low (Noca et al., 1999). Khalak and Williamson (1999) showed that by manipulating the equations of motion of a single degree of freedom cylinder, the amplitude and phase of the fluid forces can be expressed in terms of the displacement and the structural properties of the cylinder. This approach also captures the dependence of the phase difference between the fluid forces and the cylinder motion on A/D , which is often neglected in forced oscillation experiments.

This brief communication presents estimates of the fluid forces acting on a cylinder free to move only in the streamwise direction, using a similar approach to that of Khalak and Williamson (1999), in order to provide insight into the fluid excitation in streamwise vortex-induced vibrations. In particular, we seek to address the question of what causes the paradoxical reduction in vibration amplitude at resonance.

2. Experimental details

2.1. Test facilities

The experiments were performed in a closed-loop water tunnel, which has been described in detail by Konstantinidis et al. (2003) and Cagney and Balabani (2013c). It contained a $72 \text{ mm} \times 72 \text{ mm}$ test-section, which was made of Perspex, to allow optical access.

In order to support the cylinder within the flow such that it was free to move only by translation in the streamwise direction, it was suspended at either end using fishing wires. The wires were aligned normal to the cylinder axis and the

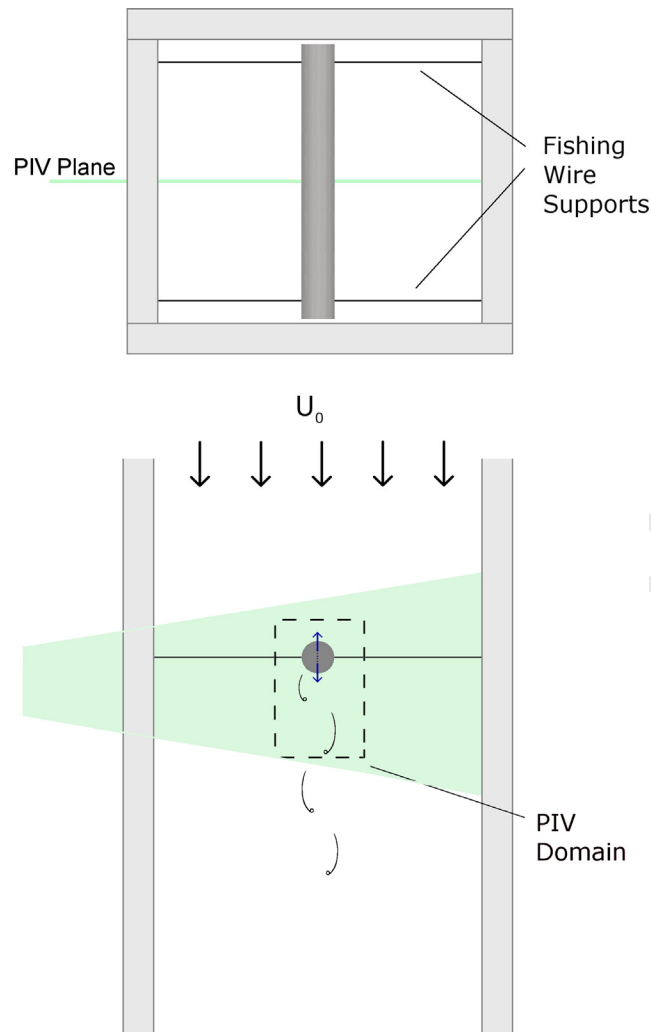


Fig. 2. Plan and elevation view of the test section used, including fishing wire supports and PIV plane.

flow direction, as shown in Fig. 2. The cylinder was held in place along the wires using silicon sealant in order to prevent any transverse motion. Great care was taken to ensure that the stiffness in both wires was approximately equal, such that the supports were balanced and any non-translational motion (i.e. pitching) was negligible (see Cagney and Balabani, 2013c for more details). The frequency spectra of the cylinder displacement signals showed that any energy occurring at sub- or super-harmonics of the primary response frequency was negligible, indicating that the stiffness of the supports was essentially linear.

The cylinder had a diameter, D , and length, L , of 7.1 mm and 71 mm, respectively. It was made of solid Perspex and had a mass ratio, $m^* = (\text{vibrating mass})/(\text{displaced fluid mass})$, of 1.17.

A series of tap tests were performed in still water to identify the natural frequency and hydrodynamic damping ratio, and a further series of tests were performed in air to identify these values in the absence of significant added mass effects (Sarpkaya, 2004). The natural frequency in water and air was $f_n = 23.7$ Hz and $f_{n,a} = 33.11$ Hz, respectively. In practice it is rarely possible to directly measure the structural damping (i.e. the damping caused by internal friction), which can only be found by performing tap tests in a vacuum (Sarpkaya, 2004). While the damping ratio measured in air, ζ_a , is often taken to represent the structural damping, the true value may be as much as an order of magnitude smaller (Sarpkaya, 2004). We therefore limit our discussion to noting that we found $\zeta_a = 0.0037$, and the tap tests in water indicated that $\zeta_w = 0.02$. Both values include the influence of the structural damping.

2.2. PIV measurements

The flow field surrounding the cylinder was measured using Particle-Image Velocimetry in order to estimate the vortex-shedding frequency and the freestream velocity. The PIV system and experimental procedure is the same as that described

in Cagney and Balabani (2013b). An Nd:Yag laser was used to illuminate the plane normal to the cylinder axis at its midspan, as shown in Fig. 2. The flow was seeded using silver-coated hollow glass spheres that had a mean diameter of 10 μm , and image-pairs were acquired using a high-speed CMOS camera (IDT X-3) and the Dynamic Studio software package (Dantec Dynamics). For each reduced velocity examined, 1000 image-pairs were acquired at 200 Hz, which corresponded to approximately 120 cylinder vibration cycles.

The streamwise and transverse spans of the PIV fields were $x/D = -1.4$ to 4.2 and $y/D = -1.65$ to 1.55, respectively, where the origin is defined as the mean cylinder position.

The cylinder position and displacement signals were estimated directly from the PIV images, using a template-matching algorithm, which has been described elsewhere (Cagney and Balabani, 2013c). The method was applied to images of a cylinder undergoing known static displacements and to images which had been binned (compressed). Based on these tests, the method was found to be accurate to within 0.4 pixels, which corresponds to 0.2% of the cylinder diameter.

The cylinder response frequency at each reduced velocity was estimated from the power-spectral-density of the displacement signal. The amplitude response was estimated from the displacement signals, which were band-pass filtered, with cut-off frequencies of 10 Hz and 40 Hz, in order to reduce the effects of noise and any low frequency oscillations that were not associated with VIV. The vibration amplitude was taken as the mean peak height of the filtered signal.

The vortex-shedding frequency, f_v , was estimated from the dominant frequency of the transverse velocity signal extracted directly from the PIV fields at $(x/D, y/D) = (3, 0)$. The values of f_v measured before the onset of lock-in ($U_r St/f^* < 0.37$) were used to estimate the Strouhal number, $St = 0.2$. PIV measurements were acquired in the reduced velocity range $U_r St/f^* = 0.19$ –0.62, which corresponded to a Reynolds number range ($Re = U_0 D/\nu$, where ν is the kinematic viscosity) of 1150–5400.

3. Force estimation

It is common to model a cylinder undergoing VIV in one direction as a simple harmonic oscillator in order to show the dependence of the vibration amplitude on various structural properties and the fluid forces (Bearman, 1984; Sarpkaya, 2004; Williamson and Govardhan, 2004). Khalak and Williamson (1999) showed that this approach can also be used to find information on the fluid forces acting on a freely oscillating cylinder if the cylinder displacement is measured.

The cylinder is assumed to have the characteristic equation of motion:

$$m\ddot{x} + c\dot{x} + kx = \tilde{F}_x(t), \quad (1)$$

where m is the mass of the cylinder, c is the damping coefficient, k is the stiffness of the system, and $\tilde{F}_x(t)$ is the fluctuating drag force. This equation can be expressed in terms of the known structural properties by dividing both sides by m (and recalling that the natural frequency in air is given by $f_{n,a} = \sqrt{k/m}/2\pi$ and the damping ratio is equal to $\zeta = c/2\sqrt{km}$);

$$\ddot{x} + 2\zeta(2\pi f_{n,a})\dot{x} + (2\pi f_{n,a})^2 x = \frac{2U_0^2}{Dm^*} \tilde{C}_D(t), \quad (2)$$

where $\tilde{C}_D = \tilde{F}_x/0.5\rho U_0^2 DL$ is the unsteady drag coefficient and ρ is the fluid density.

This approach requires a choice of damping ratio and coefficient. Khalak and Williamson (1997, 1999) used the damping measured in air, referring to it as the ‘structural damping’. However, as noted in Section 2.1, ζ_a may be larger than the true structural damping (which is not known), and neglects the role of viscous dissipation as the cylinder vibrates in water. The damping coefficient which includes these viscous effects can be found from the tap tests performed in water (which measure ζ_w and f_n) as

$$c_w = \frac{\zeta_w k}{\pi f_n}. \quad (3)$$

The damping ratio in Eq. (2) is therefore given by

$$\zeta = \frac{c_w}{2\sqrt{mk}}. \quad (4)$$

Combining these expressions we get:

$$\zeta = \left(\frac{f_{n,a}}{f_n}\right) \zeta_w = 0.0277. \quad (5)$$

The cylinder motion and unsteady drag coefficient signals are assumed to be sinusoidal, separated by a phase lag, ϕ :

$$x(t) = A \sin(2\pi f_x t), \quad (6)$$

$$\tilde{C}_D(t) = |\tilde{C}_D| \sin(2\pi f_x t + \phi). \quad (7)$$

Only the component of the fluid forcing which occurs at the cylinder response frequency will affect the steady-state response amplitude. Therefore, the assumption in Eq. (7) that the forcing occurs at f_x is less restrictive than it may at first appear; the forcing signal may contain components occurring at a range of frequencies, but $|\tilde{C}_D|$ relates only to the

1 amplitude of the component occurring at f_x . Therefore, the analysis presented here is not restricted to cases in which the
 3 fluid forcing is locked-in to the cylinder motion, but is applicable throughout the response regime. However, outside of the
 lock-in range, the estimates of the fluctuating drag will relate to the fluid forces caused by turbulent buffeting and the
 cylinder motion, rather than those caused by the vortex-shedding.

5 Eq. (6) can be differentiated to find expressions for the cylinder velocity and acceleration. Inserting these expressions and
 the relations for $x(t)$ and $\tilde{C}_D(t)$ into Eq. (2), and utilising various non-dimensional groups, the components of the unsteady
 7 drag coefficient which are in phase with the cylinder displacement and velocity can be expressed as:

$$9 \quad |\tilde{C}_D| \cos \phi = 2\pi^3 \frac{A}{D} \frac{m^*}{U_r^2} \left(\frac{f_{n,a}}{f_n} \right)^2 (1 - f_a^{*2}), \quad (8)$$

11 and

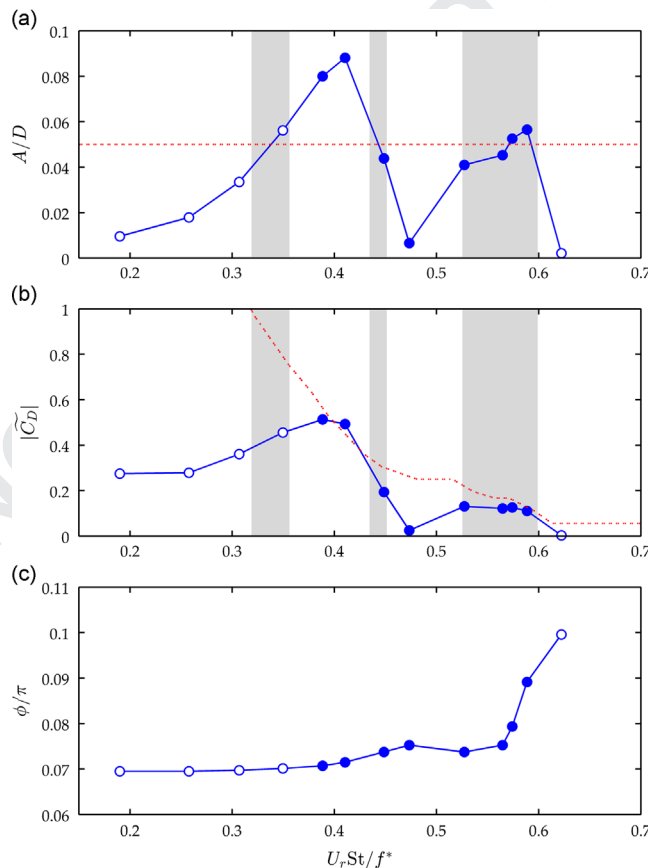
$$13 \quad |\tilde{C}_D| \sin \phi = 2\pi^3 \frac{A}{D} \frac{m^*}{U_r^2} \left(\frac{f_{n,a}}{f_n} \right)^2 (2\zeta f_a^*), \quad (9)$$

15 respectively, where $f_a^* = f_x / f_{n,a}$.

17 Eqs. (8) and (9) can be combined to produce expressions for the amplitude and phase of the fluid force:

$$19 \quad |\tilde{C}_D| = 2\pi^3 \frac{A}{D} \frac{m^*}{U_r^2} \left(\frac{f_{n,a}}{f_n} \right)^2 \sqrt{(2\zeta f_a^*)^2 + (1 - f_a^{*2})^2}, \quad (10)$$

$$23 \quad \phi = \tan^{-1} \left(\frac{2\zeta f_a^*}{1 - f_a^{*2}} \right). \quad (11)$$



27
29
31
33
35
37
39
41
43
45
47
49
51
53
55
57
59
61
Fig. 3. Amplitude response of the cylinder (a), amplitude of the fluctuating drag coefficient (b) and phase angle between the fluctuating drag and the cylinder displacement (c) throughout the streamwise response regime. The results in (b) and (c) were calculated using Eqs. (10) and (11), respectively. The dashed red lines indicate the vibration amplitude and the magnitude of $|\tilde{C}_D|$ occurring at f_x measured by Nishihara et al. (2005) for the case of a cylinder undergoing forced oscillations at $Re=34\ 000$. (For interpretation of the references to color in this figure caption, the reader is referred to the web version of this paper.)

1 Khalak and Williamson (1999) compared the estimates of the lift force acting on a transversely oscillating cylinder found
 2 from the cylinder displacement signals to those directly measured using strain gauges, for two cylinders with mass ratios of
 3 3.3 and 10.1, respectively. They found the method to be reasonably accurate for the low mass ratio cylinder, but the errors
 4 were quite large for the high m^* case; the errors in the maximum root-mean-square (rms) values of the lift force were
 5 approximately 6% and 33%, respectively (see Fig. 12 in Khalak and Williamson, 1999). They attributed this dependence of the
 6 accuracy on m^* to the difficulty in accurately measuring the frequency ratio of structures with high mass ratios, which are
 7 only weakly affected by the added-mass. In such cases f^* remains close to unity; small absolute errors in the measurement
 8 of f_x will therefore correspond to large relative errors if the formulations contain terms such as $(1-f^*)^2$ in the denominator.
 9 The formulations presented in Eqs. (10) and (11) are dependent on f_a^* (rather than f^*), which does not tend to unity at low
 10 reduced velocities. This provides a further motivation for our use of the current formulations of these equations.

11 The mass ratio of the present system is low ($m^* = 1.17$) and the changes in f_a^* were found to be relatively large ($f_a^* = 0.73$
 12 and 0.93 at the lowest and highest reduced velocities examined, respectively); therefore this method can be expected to
 13 perform reasonably well with an uncertainty comparable to that found by Khalak and Williamson for $m^* = 3.3$. However, the
 14 uncertainty may be slightly larger when f_a^* is close to unity (i.e. at high reduced velocities).

17 4. Results

19 The variation in the amplitude of the cylinder vibrations throughout the streamwise response regime is shown in
 20 Fig. 3(a). The closed symbols indicate the reduced velocities at which the vortex-shedding was found to be locked-in to the
 21 cylinder motion (i.e. the velocity fluctuations at $(x/D, y/D) = (3, 0)$ occurred at $f_x/2$). The cylinder response is characterised
 22 by two branches, separated by a low amplitude region slightly below $U_r St/f^* = 0.5$, which is consistent with previous
 23 studies examining the response of cylinders with single and multiple degrees of freedom (Aguirre, 1977; Cagney and
 24 Balabani, 2013c; Okajima et al., 2004; Jauvtis and Williamson, 2004; Blevins and Coughran, 2009). The lock-in range is
 25 $U_r St/f^* \approx 0.37-0.6$, which corresponds to the peak of the first branch, the low amplitude region and the entirety of the
 26 second branch. The first branch occurs over the range $U_r St/f^* \approx 0.25-0.45$, and has a peak amplitude of $A/D = 0.087$. The
 27 second branch has a slightly lower peak amplitude ($A/D = 0.55$), and occurs over the range $U_r St/f^* \approx 0.5-0.6$.

28 The peak of the first branch is characterised by both symmetric and alternate vortex-shedding, with the wake switching
 29 intermittently between the two modes. Instantaneous vorticity fields showing these modes at the peak of the first branch
 30 are presented in Fig. 4(a) and (b). In the second branch, the vortices are also shed alternately, with no switching between
 31 modes, and the vortices forming close to the cylinder base (Fig. 4(c)). See Cagney and Balabani (2013a,b,c) for a complete
 32 discussion of mode-switching and the variation in shedding patterns throughout the response regime.

33 The variations in the estimated amplitude and phase of the fluctuating drag coefficient found using Eqs. (10) and (11) are
 34 shown in Fig. 3(b) and (c), respectively. The amplitude of the fluctuating drag is large at low reduced velocities
 35 ($U_r St/f^* \lesssim 0.44$). A local maximum occurs at $U_r St/f^* = 0.39$, which approximately coincides with the peak of the first
 36 response branch and the onset of lock-in. Nishihara et al. (2005) also observed large amplitude fluctuating drag forces acting
 37 on a cylinder undergoing forced streamwise vibrations ($A/D = 0.05$) at low values of $U_r St/f^*$. This was also observed in the
 38 numerical simulations of Marzouk and Nayfeh (2009). By decomposing the signal into components in phase with the
 39 cylinder displacement and velocity, they showed that the large amplitude drag was caused by an increase in the inertial
 40 forces associated with the cylinder motion. Fig. 3(c) shows that the phase lag between the forcing and the displacement is
 41 low for $U_r St/f^* \lesssim 0.25$. This indicates that the fluid force acts in phase with the cylinder displacement and the inertial force
 42 acting on it (i.e. the d'Alembert force, $-m\ddot{x}$), in agreement with the results of Nishihara et al. (2005) and Marzouk and
 43 Nayfeh (2009). The magnitude of the energy transferred to the cylinder is proportional to $|\tilde{C}_D| \sin \phi$ (Khalak and Wil-
 44 liamson, 1999). Therefore, the low ϕ value indicates that in spite of the large amplitude fluctuating drag in the region
 45 $U_r St/f^* \lesssim 0.44$, the cylinder does not experience significant levels of fluid excitation, and the response amplitude
 46 remains low.

47 For $U_r St/f^* \lesssim 0.3$ the vortices are shed at the Strouhal frequency, and the cylinder does not exhibit significant vibrations.
 48 Despite the absence of lock-in, the cylinder experiences some excitation due to turbulent buffeting; therefore the cylinder
 49 response amplitude is non-zero, and Fig. 3(c) indicates that the fluid is transferring some energy to the structure (which
 50 corresponds to $\phi > 0$). Post-lock-in, when the amplitude response is negligible ($U_r St/f^* > 0.6$), the phase lag is larger,
 51 indicating a drop in the flow-induced inertial forces. As the inertial forces are low, the total amplitude of the fluctuating drag
 52 also drops to a very low value (Fig. 3(b)).

53 The dashed red line in Fig. 3(b) indicates the force measurements of Nishihara et al. (2005), obtained for a cylinder forced
 54 to oscillate in the streamwise direction at a constant amplitude of $A/D = 0.05$. The shaded regions in Fig. 3 indicate the
 55 reduced velocities at which the non-dimensional vibration amplitude was within 0.01 of the value used by Nishihara et al.
 56 (i.e. $0.04 \leq A/D \leq 0.06$). Nishihara et al. used gauges to measure the overall force acting on the oscillating cylinder, and by
 57 cross-correlating the force and the cylinder displacement signals, found the magnitude of the component on the force acting
 58 at f_x – i.e. the same quantity predicted by Eq. (10). The vibration amplitude will have a strong effect on the magnitude of the
 59 fluid forces, and the estimates of $|\tilde{C}_D|$ cannot be expected to match the measurements of Nishihara et al. when the dif-
 60 ferences in A/D are large (i.e. outside the shaded regions). However, Fig. 3(b) shows that during the lock-in range the
 61 estimates are reasonably consistent with the measured values when $A/D \approx 0.05$, in spite of the differences between the two

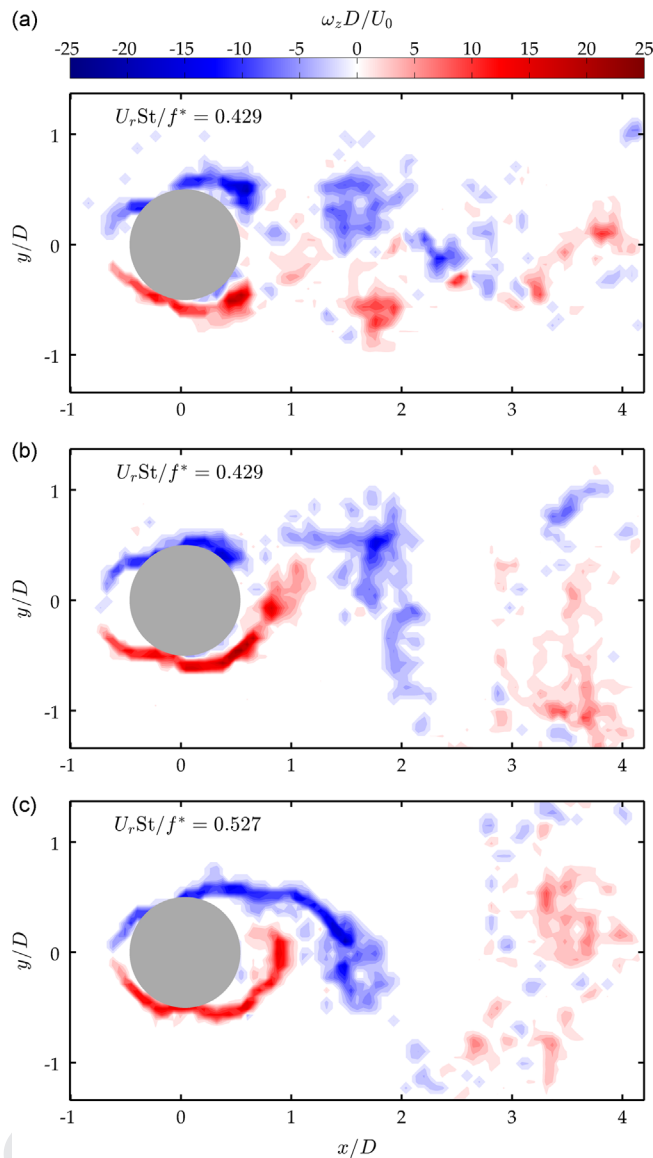


Fig. 4. Instantaneous vorticity fields showing the symmetric (a) and alternate (b) modes of vortex shedding at the peak of the first response branch ($U_r St/f^* = 0.429$), and the alternate shedding mode at the start of the second branch (c), at $U_r St/f^* = 0.527$.

studies (e.g. the use of forced/free oscillations, Re, and aspect ratio), indicating that the displacement-based method is reasonably effective. The estimates of $|\tilde{C}_D|$ found using Eq. (10) are larger than the values measured by Nishihara et al. when the response amplitude in the current study is also larger ($A/D > 0.05$), and vice versa. This is also consistent with the equations of motion, which show that the unsteady drag coefficient is dependent on the vibration amplitude, $|\tilde{C}_D| \propto A/D$ (Eq. (10)).

The phase lag between the drag and the cylinder motion does not vary significantly between the peak of the first branch and the low amplitude region at $U_r St/f^* \approx 0.5$. This indicates that the sudden decrease in the amplitude response in this region is not caused by a change in ϕ , as has been previously suggested (Nishihara et al., 2005; Konstantinidis et al., 2005). In fact, ϕ has a very small local maximum at $U_r St/f^* = 0.47$. However, there is a dramatic change in $|\tilde{C}_D|$ over this range. At $U_r St/f^* = 0.47$, $|\tilde{C}_D|$ has approximately the same amplitude as observed post-lock-in, when A/D is also negligible. This indicates that the low amplitude observed in this region is caused by a reduction in the amplitude of the fluctuating drag force, rather than a change in its phase. This is discussed further in the following section.

Within the second branch there is an increase in the amplitude of the unsteady drag coefficient, although the peak amplitude observed, $|\tilde{C}_D| = 0.13$, is considerably lower than that observed in the first branch. However, Fig. 3(c) indicates that the phase angle is larger in the second branch, which is associated with increased levels of energy transfer to the cylinder and accounts for the reasonably large levels of A/D observed in this region.

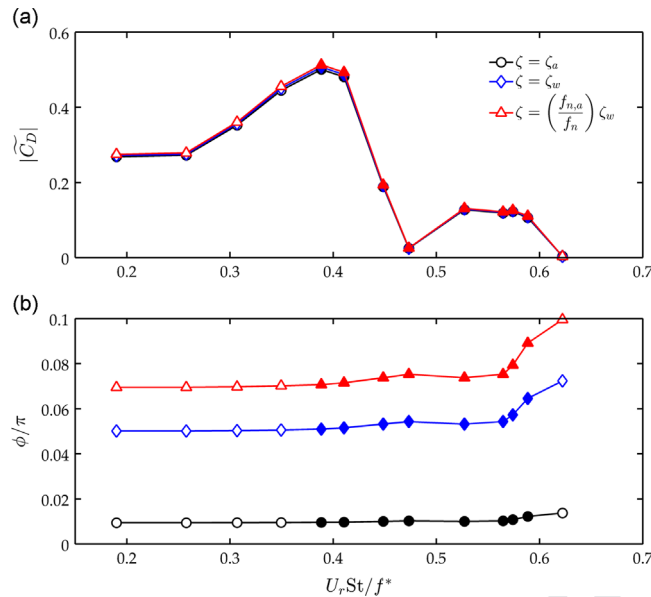


Fig. 5. Amplitude (a) and phase (b) calculated throughout the response regime for three different choices of damping ratio. Khalak and Williamson (1999) used the damping ratio measured in air (black circles), while we take into account the effect of viscous drag (red triangles). The effect on $|\tilde{C}_D|$ is negligible, while the different damping ratios cause a shift in ϕ , but do not alter its qualitative variation throughout the response regime. (For interpretation of the references to color in this figure caption, the reader is referred to the web version of this paper.)

As noted in Section 3, we define the damping ratio in terms of the damping coefficient measured in still water. In contrast, Khalak and Williamson (1997, 1999) and Govardhan and Williamson (2000) chose to use an approximation of the structural damping, based on tests performed in air. In order to study the effect of the choice of damping ratio on the estimates of the unsteady drag force, $|\tilde{C}_D|$ and ϕ were calculated for three different values of ζ : the damping ratio measured in air (as chosen by Khalak and Williamson, 1999 and Govardhan and Williamson, 2000), the damping ratio measured in water, and damping ratio given by Eq. (5).

Fig. 5(a) shows that the choice of ζ has little effect on the estimates of the amplitude of the unsteady force coefficient. This implies that the added mass term in Eq. (10) (i.e. $(1 - f_a^{*2})$ in the square root) is dominant and the component due to damping (i.e. $2\zeta f_a^*$) is relatively insignificant. However, for high mass ratio cylinders, the added mass effects are weaker and the choice of damping ratio is likely to have a significant effect on the accuracy of the estimates.

A change in the assumed value of ζ leads to a proportional increase in $\tan \phi$ (Eq. (11)), which in turn causes a corresponding increase or decrease in the estimates shown in Fig. 5(b). The increased values of ϕ for $\zeta = (f_{n,a}/f_n)\zeta_w$ (red triangles) relative to the ζ_a case (black circles) correspond to the increased force that would be required to induce a cylinder to vibration in viscous water compared to a cylinder in a vacuum. In spite of the changes in the mean values of the phase angle for each of the cases shown in Fig. 5(b), the choice of the damping ratio results in a uniform change in $\tan \phi$ throughout the response regime, and therefore does not affect the general trend; i.e. the absence of a reduction in ϕ at $U_r St / f^* \approx 0.5$, as has been predicted in previous studies.

5. Discussion and conclusions

The estimates of the unsteady drag force presented in the previous section do not support the arguments of Nishihara et al. (2005) and Konstantinidis et al. (2005) that the low amplitude region at $U_r St / f^* \approx 0.5$ is caused by a reduction in ϕ , but instead show that this region coincides with a decrease in the forcing amplitude.

It is clear from the equations of motion that the reduction in the vibration amplitude must coincide with a reduction in the phase or amplitude of the unsteady forcing, or both. Therefore, it is not sufficient to simply explain the counter-intuitive low amplitude region as being ‘caused’ by a change in $|\tilde{C}_D|$ or ϕ , which is known priori; rather the wake dynamics must be examined in order to explain what is causing the change in the fluid forcing.

One such explanation was argued by Aguirre (1977) and Okajima et al. (2004), who showed that when a splitter plate was installed behind the cylinder the low amplitude region did not occur and the first response branch continued to higher reduced velocities. At low reduced velocities in the first branch, the vortices are shed symmetrically, but the shedding becomes alternate at the peak of the first branch and throughout the low amplitude region and second branch (Fig. 4). Aguirre (1977) and Okajima et al. (2004) argued that the splitter plate prevented the alternate vortex-shedding and therefore the low amplitude region was caused by the wake transitioning to the alternate shedding mode.

Cagney and Balabani (2013a, 2014) examined the vortex-shedding at the centre-span of cylinders with one and two degrees of freedom, respectively, and showed that at a constant reduced velocity the wake mode can switch intermittently between the symmetric and alternate shedding modes, but found that this does not cause any change in the streamwise or transverse vibration amplitudes. The fact that the alternate mode does not produce a noticeable lift force is surprising given that the same mode is capable of inducing large VIV in the lift direction at other reduced velocities. Similarly, the experiments of Aguirre and Okajima et al. suggest that this change in wake mode should also result in a corresponding change in the streamwise response. These issues can be explained if the wake is highly three-dimensional in this reduced velocity range, and the shedding mode is not uniform along the cylinder span. If this is the case, the unsteady fluid forces induced by the vortex-shedding at different points along the span may destructively interfere, which may cause a reduction in $|\bar{C}_D|$ (which is averaged over the length of the cylinder) and ultimately to a reduction in A/D . In order to test this would require measurements of the three-dimensionality in the wake of a cylinder which is undergoing free or forced vibrations in the region $U_r St/f^* \approx 0.5$.

References

- Aguirre, J.E., 1977. Flow Induced, In-line Vibrations of a Circular Cylinder (Ph.D. thesis). Imperial College of Science and Technology.
- Bearman, P.W., 1984. Vortex shedding from oscillating bluff bodies. *Annual Review of Fluid Mechanics* 16, 195–222.
- Blevins, R.D., Coughran, C.S., 2009. Experimental investigation of vortex-induced vibrations in one and two dimensions with variable mass, damping, and Reynolds number. *Journal of Fluids Engineering* 131 (101202), 1–7.
- Cagney, N., Balabani, S., 2013a. Mode competition in streamwise-only vortex induced vibrations. *Journal of Fluids and Structures* 41, 156–165.
- Cagney, N., Balabani, S., 2013b. On multiple manifestations of the second response branch in streamwise vortex-induced vibrations. *Physics of Fluids* 25 (075110), 1–17.
- Cagney, N., Balabani, S., 2013c. Wake modes of a cylinder undergoing free streamwise vortex-induced vibrations. *Journal of Fluids and Structures* 38, 127–145.
- Cagney, N., Balabani, S., 2014. Streamwise vortex-induced vibrations of cylinders with one and two degrees of freedom. *Journal of Fluid Mechanics* 758, 702–727.
- Govardhan, R., Williamson, C.H.K., 2000. Modes of vortex formation and frequency response of a freely vibrating cylinder. *Journal of Fluid Mechanics* 420, 85–130.
- Jauvtis, N., Williamson, C.H.K., 2003. Vortex-induced vibration of a cylinder with two degrees of freedom. *Journal of Fluids and Structures* 17, 1035–1042.
- Jauvtis, N., Williamson, C.H.K., 2004. The effect of two degrees of freedom on vortex-induced vibration at low mass and damping. *Journal of Fluid Mechanics* 509, 22–63.
- Khalak, A., Williamson, C.H.K., 1997. Investigation of relative effects of mass and damping in vortex-induced vibration of a circular cylinder. *Journal of Wind Engineering and Industrial Aerodynamics* 69–71, 341–350.
- Khalak, A., Williamson, C.H.K., 1999. Motions, forces and mode transitions in vortex-induced vibrations at low mass-damping. *Journal of Fluids and Structures* 13, 813–851.
- Konstantinidis, E., 2014. On the response and wake modes of a cylinder undergoing streamwise vortex-induced vibrations. *Journal of Fluids and Structures* 45, 256–262.
- Konstantinidis, E., Balabani, S., Yianneskis, M., 2003. The effect of flow perturbations on the near wake characteristics of a circular cylinder. *Journal of Fluids and Structures* 18, 367–386.
- Konstantinidis, E., Balabani, S., Yianneskis, M., 2005. The timing of vortex shedding in a cylinder wake imposed by periodic inflow perturbations. *Journal of Fluid Mechanics* 543, 45–55.
- Konstantinidis, E., Liang, C., 2011. Dynamic response of a turbulent cylinder wake to sinusoidal inflow perturbations across the vortex lock-on range. *Physics of Fluids* 23 (075102), 1–21.
- Marzouk, O.A., Nayfeh, A.H., 2009. Reduction of loads on a cylinder undergoing harmonic in-line motion. *Physics of Fluids* 21 (083103), 1–13.
- Morse, T.L., Williamson, C.H.K., 2009. Prediction of vortex-induced vibration response by employing controlled motion. *Journal of Fluid Mechanics* 634, 5–39.
- Nishihara, T., Kaneko, S., Watanabe, T., 2005. Characteristics of fluid dynamic forces acting on a circular cylinder oscillating in a streamwise direction and its wake patterns. *Journal of Fluids and Structures* 20, 505–518.
- Noca, F., Shiels, D., Jeon, D., 1999. A comparison of methods for evaluating time-dependent fluid dynamic forces on bodies, using only velocity fields and their derivatives. *Journal of Fluids and Structures* 13, 551–578.
- Okajima, A., Nakamura, A., Kosugi, T., Uchida, H., Tamaki, R., 2004. Flow-induced in-line oscillation of a circular cylinder. *European Journal of Mechanics B/Fluids* 23, 115–125.
- Sarpkaya, T., 2004. A critical review of the intrinsic nature of vortex-induced vibrations. *Journal of Fluids and Structures* 19, 389–447.
- Williamson, C.H.K., Govardhan, R., 2004. Vortex-induced vibrations. *Annual Review of Fluid Mechanics* 36, 413–455.
- Williamson, C.H.K., Roshko, A., 1988. Vortex formation in the wake of an oscillating cylinder. *Journal of Fluids and Structures* 2, 355–381.